

# Basic principles of electrolyte chemistry for microfluidic electrokinetics.

## Part II:† Coupling between ion mobility, electrolysis, and acid–base equilibria‡

Alexandre Persat,§ Matthew E. Suss§ and Juan G. Santiago\*

Received 1st April 2009, Accepted 4th June 2009

First published as an Advance Article on the web 7th July 2009

DOI: 10.1039/b906468k

We present elements of electrolyte dynamics and electrochemistry relevant to microfluidic electrokinetics experiments. In Part I of this two-paper series, we presented a review and introduction to the fundamentals of acid–base chemistry. Here, we first summarize the coupling between acid–base equilibrium chemistry and electrophoretic mobilities of electrolytes, at both infinite and finite dilution. We then discuss the effects of electrode reactions on microfluidic electrokinetic experiments and derive a model for pH changes in microchip reservoirs during typical direct-current electrokinetic experiments. We present a model for the potential drop in typical microchip electrophoresis device. The latter includes finite element simulation to estimate the relative effects of channel and reservoir dimensions. Finally, we summarize effects of electrode and electrolyte characteristics on potential drop in microfluidic devices. As a whole, the discussions highlight the importance of the coupling between electromigration and electrophoresis, acid–base equilibria, and electrochemical reactions.

### Introduction

Electrode chemistry, acid–base chemical equilibria, and ionic strength have a significant effect on the performance of microfluidic electrokinetic devices. Among other effects, these

characteristics determine local electroosmotic flow mobilities,<sup>1,2</sup> shapes of electropherograms,<sup>2</sup> conductivity and power consumption,<sup>3</sup> and compatibility with chemical and biological species.<sup>4</sup> In typical direct current (DC) electrokinetic (EK) systems, passive DC electrodes are inserted into end-channel reservoirs which have characteristic dimensions relatively large compared to those of microchannels.<sup>5,6</sup> Faradaic current (electron transfer to and from electrodes) and ionic (Ohmic) current together sustain an electric field in the bulk of the electrolyte. The rate and nature of electrolytic reactions can strongly influence the acid–base equilibria (including pH) at channel reservoirs and in the channel itself. In turn, these acid–base equilibria determine local ion mobilities and conductivities of the electrolyte, and so

Department of Mechanical Engineering, Stanford University, Stanford, CA, 94305, USA. E-mail: [juan.santiago@stanford.edu](mailto:juan.santiago@stanford.edu); Fax: +1 650-723-5689; Tel: +1 650-723-7657

† For Part I see ref. 7.

‡ Part of a *Lab on a Chip* themed issue on fundamental principles and techniques in microfluidics, edited by Juan Santiago and Chuan-Hua Chen.

§ The first two authors contributed equally to this work.



Alexandre Persat is a PhD candidate at Stanford University, under the supervision of Prof. Juan G. Santiago. He received his MS in Chemical Engineering at Stanford University, and his Diplôme d'Ingénieur from l'Ecole Polytechnique, France.



Matthew E. Suss received his B. Eng degree in Mechanical Engineering from McGill University, Montreal, in 2007. Currently, he is finishing a M.Sc. at Stanford University, Stanford, CA where his research has been supported by an FQRNT fellowship from the Quebec government. His work in the Stanford Microfluidics Laboratory focuses on the development of highly efficient electroosmotic micropumps for drug delivery applications.

Matthew additionally spent two summers as an undergraduate research assistant working on three-dimensional characterization of osseous implant surface topography.

reactions occurring at the electrode surfaces are intimately coupled to local chemistry and electrokinetic phenomena.

In Part I of this two-paper series,<sup>7</sup> we presented elements of acid–base equilibrium chemistry and pH buffering, and we discussed their importance to microfluidic electrokinetic experiments. In this second paper, we present an introduction to the basic principles of the coupling between electrolyte mobilities, acid–base equilibria, and electrolysis in typical DC EK systems. We first present a summary of the effects of ionic strength and pH on (observable) effective electrophoretic mobilities. As with Part I, we first summarize dilute approximations and then discuss extrapolation to finite ionic strength. We characterize conductivity in terms of these effective mobilities. We then summarize the coupling between ionic conductivity, system geometry, and electrolytic reaction rates. We analyze typical electrolyte systems to demonstrate and summarize the effects of electrolysis on end-channel pH values. We additionally analyze electrolytic and Ohmic sources of potential loss, which may aid in design of EK systems. Our intent is to provide an introductory review of principles, provide citations for key phenomena, and summarize various illustrative analyses.

#### Nonemclature

$e^-$	electron
$c_X$	analytical concentration of X
$c_{X,z}$	concentration of X in valence state $z$ (M)
$d$	Microchannel diameter (m)
$D$	Reservoir diameter (m)
$E_{eq}$	Equilibrium potential (V)

$F$	Faraday's constant $\approx 96485$ C mol <sup>-1</sup>
$f$	Transport (or transference) number
$g_{A,z}$	Fraction of A in valence state $z$
$i$	Current (A)
$I$	Ionic strength (M)
$j_{o,a}$	Anode exchange current density (A m <sup>-2</sup> )
$J_X^c$	Flux of X in anode/cathode reservoir
$K_a$	Acid dissociation constant
$L$	Channel length (m)
$L_{eff}$	Effective length of reservoir (m)
$S_{eff}$	Effective cross sectional area of reservoir (m <sup>2</sup> )
$S$	Channel cross sectional area (m <sup>2</sup> )
$n_X$	Minimum valence of species X
$p_X$	Maximum valence of species X
$V_{app}$	Applied potential (V)
$V_c$	Potential across microchannel (V)
$V_{res}$	Potential drop across reservoir (V)
$\gamma$	Ratio of anode to cathode reservoir conductivities
$\gamma_X$	Activity coefficient of species X
$\gamma_{\pm}$	Mean activity coefficient of a cation/anion pair
$\phi$	Local potential (V)
$\mu_X$	Effective electrophoretic mobility of X (m <sup>2</sup> V <sup>-1</sup> s <sup>-1</sup> )
$\mu_{X,z}^o$	Fully ionized mobility of X <sup>z</sup> (m <sup>2</sup> V <sup>-1</sup> s <sup>-1</sup> )
$\mu_{X,z}^{\infty}$	Mobility of X <sup>z</sup> at zero ionic strength (m <sup>2</sup> V <sup>-1</sup> s <sup>-1</sup> )
$\eta_{ac}$	Anode/cathode overpotential (V)
$\sigma$	Conductivity (S m <sup>-1</sup> )
$Y$	Reservoir volume (m <sup>3</sup> )



*Prof. Juan G. Santiago is an Associate Professor in the Mechanical Engineering Department at Stanford, and specializes in microscale transport phenomena and electrokinetics. He received his MS and PhD in Mechanical Engineering from the University of Illinois at Urbana-Champaign (UIUC). His research includes the development of microsystems for on-chip electrophoresis, drug delivery, sample concentration methods, and miniature fuel*

*cells. He has received a Frederick Emmons Terman Faculty Fellowship ('98–'01); won the National Inventor's Hall of Fame Collegiate Inventors Competition ('01); was awarded the Outstanding Achievement in Academia Award by the GEM Foundation ('06); and was awarded a National Science Foundation Presidential Early Career Award for Scientists and Engineers (PECASE) ('03–'08). Santiago has given 13 keynote and named lectures and more than 100 additional invited lectures. He and his students have been awarded nine best paper and best poster awards. Since 1998, he has graduated 14 PhD students and advised 10 postdoctoral researchers. He has authored and co-authored 95 archival publications, authored and co-authored 190 conference papers, and been awarded 25 patents.*

## Effective mobility

In the Background section of Part I, we presented fairly general expressions for chemical equilibrium based on activity coefficients. We recall that activity coefficients represent the link between experimentally accessible quantities (*i.e.*, species concentrations) and the energetics of equilibrium reactions (*i.e.*, through chemical potentials).<sup>8</sup> In particular, we noted activity coefficients strongly depend on ionic strength. We also presented a general treatment of acid–base equilibrium reactions, and derived general expressions for concentrations of species in their various protonated states, as a function of pH and dissociation constants. In this section, we will first discuss the effects of acid–base equilibrium on electrophoretic transport coefficients of species. We will then relax the assumption of ideal dilute solutions and summarize the effects of ionic strength on ionic transport.

### Effective mobility of a partially ionized weak electrolyte ion

In this section, we present relations applicable to the electrophoretic transport of multi-ion systems. The discussion applies to both weak and strong electrolytes and is crucial to the control and interpretation of experiments and measurements which depend on ion mobility. Such applications include capillary zone electrophoresis, isotachopheresis, isoelectric focusing, field

amplified sample stacking, and a wide variety of other electrokinetic techniques.<sup>9,10</sup> We here restrict our discussion to electromigration in free solution (*e.g.*, versus electromigration of macromolecules through gels).

We here define ion mobility as in most electrophoresis applications as the proportionality constant between observed ion velocity and electric field (a signed quantity).<sup>11</sup> Electrophoretic mobility is typically quantified by capillary electrophoresis.<sup>9</sup> The time-averaged mobility of a species in solution can be related to the fraction of time the species spends in its various relevant ionization states. For observation times much longer than the time scales associated with proton exchange reactions (typically very short<sup>11</sup>), we observe an “effective mobility” which is the time average of the fully ionized mobilities associated with each ionization state. For a simple monovalent weak acid, the mobility of the species X of analytical concentration  $c_X = c_{X,0} + c_{X,-1}$  at a given pH is then:<sup>12</sup>

$$\mu_X = \alpha_X \mu_{X,-1}^o. \quad (1)$$

Here  $\alpha_X = c_{X,-1}/c_X$  is the degree of dissociation of the acid X, and  $\mu_{X,-1}^o$  is the fully ionized mobility of  $X^-$  (the superscript *o* indicates an ideal state where the ion is always charged at the valence described by the second subscript¶). Our notation follows the conventions we established in Part I; so  $c_{X,-1}$  and  $c_X$  are respectively equal to the concentration of species X in the  $z = -1$  valence state and the total concentration of X (summed over all ionization states). More generally, for species X with several ionization states, the motion in response to an electric field is described as follows:

$$\vec{u} = \mu_X \vec{E} = \left( \sum_{z=n_X}^{p_X} \mu_{X,z}^o g_{X,z} \right) \vec{E}, \quad (2)$$

where  $E\vec{p}$  is the local applied electric vector field and  $u\vec{p}$  is the electrophoretic velocity vector of the species. This velocity describes the time-averaged transport associated with all valences of the species family X (here “family” includes all ionization states of X).  $\mu_{X,z}^o$  is the fully ionized mobility corresponding specifically to the charge state  $z$ . We define  $g_{X,z}$  as the fraction of X in charge state  $z$ :

$$g_{X,z} \equiv \frac{c_{X,z}}{c_X} = \frac{L_{X,z} c_H^z}{\sum_{z=n_X}^{p_X} L_{X,z} c_H^z}, \quad (3)$$

where  $L_{X,z}$  was defined in Part I. Note that the degree of dissociation,  $\alpha_X$ , is the sum of  $g_{X,z}$  over all  $z \neq 0$ . Accordingly, the effective mobility of X is given by:

$$\mu_X = \sum_{z=n_X}^{p_X} \mu_{X,z}^o g_{X,z}. \quad (4)$$

$\mu_X$  is the mobility which is directly observable and quantified in a uniform pH and uniform ionic strength capillary zone

¶  $\mu_{X,z}^o$  is directly observable in electrophoresis type experiments only if there is a pH where the species exists predominantly in the valence state  $z$  (*i.e.*, such that  $c_{X,z} \cong c_X$ ). For example, direct observation of a divalent acid mobility value  $\mu_{X,-1}^o$  is not possible if  $K_{X,-2}$  is less than  $\sim 10$  fold lower than  $K_{X,-1}$ .

electrophoresis experiment. In the case of a monovalent acid (with only one relevant  $pK_a = pK_{X,-1}$ ) and a fully ionized mobility  $\mu_{X,-1}^o$ , we obtain  $L_{X,0} = 1$ ,  $L_{X,-1} = K_{X,-1}$  (see Part I) so that:

$$g_{X,0} = \frac{1}{1 + K_{X,-1}/c_H}$$

and

$$g_{X,-1} = \frac{K_{X,-1}/c_H}{1 + K_{X,-1}/c_H}.$$

Since the mobility of a neutral species is zero, we have

$$\begin{aligned} \mu_X &= \underbrace{\mu_{X,0}^o}_{=0} g_{X,0} + \mu_{X,-1}^o g_{X,-1} = \mu_{X,-1}^o \frac{1}{1 + c_H/K_{X,-1}} \\ &= \mu_{X,-1}^o \frac{1}{1 + 10^{pK_{X,-1} - \text{pH}}}. \end{aligned} \quad (5)$$

Note here the importance of dissociation states on the observed mobility of a monovalent acid. For example, fully ionized mobilities of monovalent acids ( $z = -1$ ) range from roughly  $-20 \times 10^{-9} \text{ m}^2 \text{ V}^{-1} \text{ s}^{-1}$  to  $-35 \times 10^{-9} \text{ m}^2 \text{ V}^{-1} \text{ s}^{-1}$  (*e.g.*, among the Good’s buffer ions); a range with a maximum-to-minimum ratio of roughly  $\sim 2$ . In contrast, the ratio  $c_H/K_{X,-1}$  can vary by more than 2 orders of magnitude in practice; and so the observed mobility of a monovalent acid varies between 0 and its fully ionized value.

As a second example, we provide the effective mobility,  $\mu_X$ , of a divalent acid with two  $pK_a$ ’s and corresponding valences of  $-2$  and  $-1$ . For this case,  $L_{X,0} = 1$ ,  $L_{X,-1} = K_{X,-2}$  and  $L_{X,-2} = K_{X,-2}K_{X,-1}$ ; and the effective electrophoretic mobility of this acid X is

$$\mu_X = \frac{\mu_{X,-1}^o + \mu_{X,-2}^o 10^{\text{pH} - pK_{X,-2}}}{1 + 10^{\text{pH} - pK_{X,-2}} + 10^{pK_{X,-1} - \text{pH}}}. \quad (6)$$

Relations for effective mobilities of other multivalent species, including mono- and di-valent weak bases, follow easily from this approach to the formulation.

### Back-of-the-envelope estimates for monovalent weak acids and bases

For a simple acid with a single relevant  $pK_{-1}$  ( $\text{HA} \rightleftharpoons \text{A}^- + \text{H}^+$ ), inspection of equation (5) above yields the intuitive results that

- If  $\text{pH} \ll pK_{-1}$ ,  $\mu_X \approx 0$
- If  $\text{pH} \approx pK_{-1}$ ,  $\mu_X \approx \mu_{X,-1}^o/2$
- If  $\text{pH} \gg pK_{-1}$ ,  $\mu_X \approx \mu_{X,-1}^o$

Conversely, for weak bases with ionization states 0 (base) and  $+1$  (acid) and acid dissociation constant  $pK_{+1}$  ( $\text{BH}^+ \rightleftharpoons \text{B} + \text{H}^+$ ), we write similarly

- If  $\text{pH} \gg pK_{+1}$ ,  $\mu_X \approx 0$
- If  $\text{pH} \approx pK_{+1}$ ,  $\mu_X \approx \mu_{X,+1}^o/2$
- If  $\text{pH} \ll pK_{+1}$ ,  $\mu_X \approx \mu_{X,+1}^o$

Although very useful as reference points, we caution the reader not to employ linear interpolations between these points due to the exponential nature of pH and  $pK_{-1}$ .

### Back-of-the-envelope calculations for two weak electrolytes in a buffer

Consider again the example of a pH buffer containing a weak acid HA and a weak base B. The relevant equilibrium reactions were  $HA \rightleftharpoons A^- + H^+$  and  $BH^+ \rightleftharpoons B + H^+$ . If the  $pK_a$  values of these electrolytes are sufficiently far from each other (say a value of 2 or greater), then the calculations of mobilities can be simplified. If the buffer is sensibly titrated to, say,  $pH = pK_{HA,-1} < pK_{B,+1} - 2$ , then we can assume the base B is fully ionized. Therefore,  $c_{HA,-1} \cong c_{HA}/2$  and  $c_{B,1} \cong c_B$ . Accordingly, the effective mobilities are simply  $\mu_{HA} \approx \mu_{HA,-1}^0/2$  and  $\mu_B \approx \mu_{B,+1}^0$ .

### Transference number and conductivity

Effective ion mobilities determine time-average electrophoretic velocities of ions in solutions, their respective contributions to total current, and overall ionic conductivity. Two important relations follow from these formulations. First, we define the ionic conductivity in the usual way as

$$\sigma = F \sum_X \sum_z z \mu_{X,z}^0 c_{X,z}, \quad (7)$$

where  $F$  is Faraday's constant, and  $c_{X,z}$  the concentration of X in valence state  $z$ . The summation is performed over all species in solution (*i.e.*, over all valences of all families). Note that conductivity is a function of local acid–base equilibria through  $c_{X,z}$ .

As an illustrative example, we summarize here the conductivity of a simple weak acid buffer HA titrated with a strong base B. The relevant equilibrium reaction is  $HA \rightleftharpoons A^- + H^+$ . The conductivity of the solution is then

$$\sigma = F(\mu_{B,+1}^0 c_{B,+1} + \mu_{H^+}^0 c_{H^+} - \mu_{A,-1}^0 c_{A,-1} - \mu_{OH^-}^0 c_{OH^-}). \quad (8)$$

This expression simplifies when assuming that the current carried by hydronium and hydroxide ions is small compared to the solutes. Under this assumption (sometimes called the “safe pH” approximation<sup>13</sup>), the conductivity is approximately:

$$\sigma = F(\mu_{B,+1}^0 c_{B,+1} - \mu_{A,-1}^0 c_{A,-1}), \quad (9)$$

where the weak electrolyte ion species concentration obviously depends on pH. For example, if  $c_A$  is the weak acid concentration, then:

|| The “safe pH” approximation is more restrictive than the “moderate pH” approximation.<sup>7</sup> The electrophoretic mobilities of hydronium and hydroxide ions are large. Even at small concentrations, these ions can carry a large portion of the current. Therefore, in the safe pH approximation, concentrations of hydronium and hydroxide ions need to be significantly smaller than in the moderate pH approximation. The safe pH approximation applies to the pH range 5–9 for electrolytes with concentrations on the order of 10 mM.<sup>13</sup>

$$\sigma = \frac{Fc_A}{1 + 10^{pK_a - pH}} (\mu_{B,+1}^0 - \mu_{A,-1}^0). \quad (10)$$

A second quantity which we shall leverage below is the transference number (or transport number) of species X,  $f_X$ , defined as:

$$f_X = \frac{F\mu_X c_X}{\sigma}, \quad (11)$$

where  $\mu_X$  is the effective electrophoretic mobility of X, and  $c_X$  is the analytical concentration of X. The transference number indicates the relative contribution of a species to the total current. Note that, in a binary electrolyte, the transference number of the cation and anion are not necessarily equal, as these don't necessarily have precisely equal effective mobilities. It is a quantity intertwined with the history of electrophoresis<sup>14</sup> as individual ion contributions to current (and their effective mobility) can be determined by comparing the conductivity of electrolytes.<sup>8</sup> More importantly, transference number is particularly useful in displacement processes such as isotachopheresis,<sup>15</sup> moving boundary electrophoresis,<sup>16,17</sup> and isoelectric focusing.<sup>18,19</sup>

In Part I, we saw that  $pK_a$  is a function of ionic strength through charge shielding effects. In the next section, we will discuss how fully-ionized mobility  $\mu_{X,z}^0$  is also a function of ionic strength.

### Mobilities at finite dilution: Effect of ionic strength

We here summarize the dependence of electrophoretic mobility on ionic strength. We also provide several practically useful equations we can leverage to design and optimize electrokinetic processes. The effect of ionic strength on electrokinetic experiments (*e.g.*, the shape and interpretation of electropherograms) can be significant and yet these are often ignored. General modeling of the phenomena is complex and numerous models have been developed, many of which require species-specific empirical or approximate parameters. In our opinion, the best treatment of this theory can be found in the book by Robinson and Stokes,<sup>8</sup> although there are many and more recent publications.<sup>12</sup> Further, in modeling electrokinetic systems, ionic strength couples with solution composition. This typically requires iterative resolution schemes (*e.g.*, to solve for conductivity) and always makes analytical models more complex.

We recall that ionic strength,  $I$ , is defined as  $I = (1/2) \sum z^2 c_{X,z}$ . In the current context,  $I$  can be interpreted as a measure of the deviation from the infinite dilution approximation. At finite high ionic strength, each ion is surrounded by a counterion atmosphere with dimensions on the order of the Debye screening length  $\lambda_D$ .<sup>8</sup> Ionic strength then affects electrophoretic mobility through two distinct mechanisms. First, there is a hydrodynamic phenomenon called the electrophoretic effect associated with the drag force which the (moving) counter ions exert on the respective ion.<sup>8</sup> Second is an electrodynamic effect called the relaxation effect. The latter is associated with the polarization of the counterion atmosphere which reduces the (local) electric field experienced by the ion.<sup>8</sup> Both effects act to reduce the electrophoretic velocity of the ion.

We here suggest a correction for electrophoretic mobilities which we have found to be a useful trade-off between accuracy and simplicity. The Pitts equation as suggested by Li *et al.*<sup>12</sup> includes ionic strength and finite-radius effects and is valid for binary electrolytes. In water at 25 °C, the Pitts equation becomes:

$$\mu_{X,z}^o = \mu_{X,z}^\infty - \left( 3.1 \times 10^{-4} z + 0.39 |z| |z_{ci}| \frac{2q}{1 + \sqrt{q}} \mu_{X,z}^\infty \right) \frac{\sqrt{I}}{1 + 0.33 a \sqrt{I}} \quad (12)$$

where  $\mu_{X,z}^\infty$  is the ion mobility at infinite dilution (*i.e.*, at  $I = 0$ ) expressed in equation (12) in  $\text{cm}^2 \text{V}^{-1} \text{s}^{-1}$ ,  $z_{ci}$  is the valence of the counterion, and  $a$  is an effective atomic radius given in Å. Finding data on effective atomic radii remains difficult for compounds other than small ions and an obstacle to accurate mobility prediction. For small ions, there are several relevant references for parameter  $a$ .<sup>20</sup> The value of  $a$  typically varies between about 3 and 10 Å. The parameter  $q$  depends on the infinite dilution value of counterion mobility,  $\mu_{ci,z}^\infty$ , as follows:

$$q = \frac{|zz_{ci}|}{|z| + |z_{ci}|} \frac{\mu_{X,z}^\infty + \mu_{ci,z}^\infty}{|z| \mu_{X,z}^\infty + |z_{ci}| \mu_{ci,z}^\infty} \quad (13)$$

For example, for a symmetric (binary) electrolyte,  $q = 1/2$ . Note that the Pitts equation is strictly valid for binary electrolytes. The Fuoss-Onsager correction is more adapted to mixtures of an arbitrary number of ionic species.<sup>21</sup>

We can combine equations (12) and (4) to derive the effective mobility of a weak electrolyte at finite ionic strength. Note that, in most cases, the concentration ratios  $g_{X,z}$  in (4) are functions of  $pK$ 's.  $pK$ 's are intimately (and mathematically implicitly) coupled to ionic strength. That is, ionic strength determines  $pK$  values (*e.g.*, through the Davies equation described in Part I).  $pK$  values, in turn, determine ionization states and therefore ionic strength. Hence, estimating actual mobility values almost always requires numerical, iterative solutions. In Part I, we summarize various computational tools available online to determine acid–base equilibria and ionic-strength-dependent effective mobilities.

In Fig. 1, we show typical calculations leveraging these two models. Shown is the electrophoretic mobility of fluorescein, arguably the most common (and inexpensive) fluorescent dye used in microfluidics, as a function of pH and increasing values of ionic strength. The calculations assume that ionic strength and pH are set by a background electrolyte (so that fluorescein does not participate in ionic strength or buffering here, and this greatly simplifies expression for its mobility). We assume the relevant  $pK$  values and mobilities of fluorescein reported by Whang and Yeung<sup>22</sup> and Mchedlov-Petrosyan *et al.*<sup>23</sup> and Milanova *et al.*<sup>24</sup> The largest variations of mobility are due largely to the strong effects of ionization states discussed earlier. Fluorescein has infinite dilution  $pK$  values of 4.45 and 6.8 for valence pairs of (0, -1) and (-1, -2), respectively. The respective values of  $pK_{-1}$  and  $pK_{-2}$  change by about 0.21 and 0.43  $pK_a$  units from 0 to 100 mM ionic strength (respectively, by 0.27 and 0.54 units from 0 to 500 mM). For a fixed pH value, the mobility decreases with ionic strength as the electrophoretic and relaxation effects discussed above become increasingly more important. Overall, we see that fluorescein mobility is a strong function

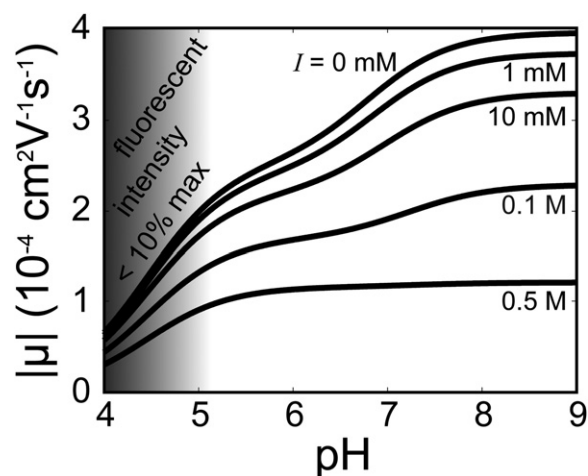


**Fig. 1** Ionic strength and pH effects on electrophoretic mobility of fluorescein. We use the Pitts equation (equation (12)) and Davies equations (eq. (40) of Part I of this two-paper series) to correct electrophoretic mobility and  $pK_a$  for ionic strength effects, respectively. We plot the absolute value of fluorescein mobility (all values are actually negative). The values of concentrations correspond to ionic strength of the solution, and the concentration of fluorescein is small compared to ionic strength. We used sodium as counterion. The dissociation coefficients of fluorescein yield the strongest influence of pH on mobility according to equations (6). The shaded zone corresponds to pH values where fluorescein fluorescence is below 10% its maximum value.<sup>25,26</sup> We used  $pK_{-1} = 4.45$ ,  $pK_{-2} = 6.8$ ,<sup>26</sup> and  $\mu_{-2} = -39.5 \times 10^{-9} \text{ m}^2 \text{ V}^{-1} \text{ s}^{-1}$  and  $\mu_{-1} = -25 \times 10^{-9} \text{ m}^2 \text{ V}^{-1} \text{ s}^{-1}$ ,<sup>23,24</sup> and  $a = 4 \text{ Å}$ . In the electrophoretic mobility calculations, we neglected the effect of the cationic form of fluorescein ( $pK_1 = 2.1$ ).

of electrolyte chemistry. For example, fluorescein mobility at pH 5 and 100 mM ionic strength is  $-11.6 \times 10^{-9} \text{ m}^2 \text{ V}^{-1} \text{ s}^{-1}$ ; as compared to a value of  $-37.3 \times 10^{-9} \text{ m}^2 \text{ V}^{-1} \text{ s}^{-1}$  at pH 8 and 1 mM. We note that fluorescein's quantum yield (which determines fluorescence intensity) drops quickly for pH below about 5,<sup>25,26</sup> and we indicate this in the plot with a shaded region.

### Summary of ionic strength effects on $pK_a$ and fully ionized electrophoretic mobility

In Part I, we summarized the effects of ionic strength on acid dissociation constants,  $pK$ 's. In particular, we proposed a (rather typical) Davies equation model (equation (40) of Part I) to correct acid–base dissociation constants for ionic strength. Above, we summarized how  $pK$  values strongly influence the effective ion mobility of an arbitrary species. We saw how  $pK$  values determine effective ion mobility by determining the prevalence of ionic states and their associated fully-ionized mobility (see eqs. (6) above). Further, we presented a correction of the dilute approximation for fully-ionized electrophoretic mobilities. Namely, we advised use of the Pitts equation to approximate  $\mu_{X,z}^o$  from  $\mu_{X,z}^\infty$  (see equation (12)). We then summarized how to determine effective mobilities for both corrected dissociation constants,  $pK$ 's, and corrected fully-ionized mobilities,  $\mu_{X,z}^o$  (see eqs. (4) and (12)). In Table 1, we summarize these derivations and the various applications of concentrations *versus* activities in both dilute and non-dilute solutions for dissociation constants, mobilities, and conservation equations.

**Table 1** Summary of example uses of activity and/or concentration in chemistry and mass transport equations. The 4<sup>th</sup> column gives examples of corrections when applicable

Equation	Formulation for ideal, infinite dilution case (and example case)	Actual dependence (and example case)	Corrections (and example case)
Chemical equilibrium <sup>a</sup> (law of mass action) (monovalent acid)	Concentrations $K_{X,-1}^{\infty} = c_H c_{X,-1} / c_{X,0}$	Activities $K_{X,-1} = K_{X,-1}^{\infty} \gamma_{\pm}^2 = c_H c_{X,-1} / c_{X,0}$	Davies (see Part I) $\Delta pK_{X,-1} = pK_{X,-1}^{\infty} - pK_{X,-1}$ $= -1.02(1-z)(\sqrt{I}/(1+\sqrt{I}) - 0.3I)$
Conservation equations	Concentrations $c_X = c_{X,0} + c_{X,-1}$ (monovalent acid)	Concentrations $c_X = c_{X,0} + c_{X,-1}$ (monovalent acid)	NA
pH	Concentrations $\text{pH} = -\log_{10} c_H$ (hydronium concentration)	Activities $\text{pH} \equiv -\log_{10}(\gamma_H c_H)$ (hydronium concentration)	Depends on pH electrode and standard. Refer to Galster <sup>30</sup> or Butler and Cogley <sup>31</sup> for discussion on pH scales. See Levine <sup>1</sup> chapter 23
Kinetic rate definition (for the reaction $X + Y \rightarrow XY$ ) <sup>11</sup>	Concentrations <sup>11</sup> $-\frac{dc_X}{dt} = k^{\infty} c_X c_Y$	Activities <sup>11</sup>	
Electrophoretic mobilities: Strong electrolyte	Infinite dilution mobility: $\mu_{X,z}^{\infty}$	Finite dilution mobility: $\mu_{X,z}$	Pitts equation <sup>12</sup> for 1:1 electrolyte $\mu_{X,z}^0 = \mu_{X,z}^{\infty} - (3.1 \times 10^{-4} + 0.16\mu_{X,z}^{\infty}) \frac{\sqrt{I}}{1 + 0.33a\sqrt{I}}$
Electrophoretic mobilities: Weak electrolyte	Concentrations in terms of $g_{X,z}$ , infinite dilution $pK_a$ , and infinite dilution mobility $\mu_{X,z}^{\infty}$ <sup>28</sup> Concentrations <sup>28</sup> $\frac{Dc_{X,z}}{Dt} = \nabla \cdot (\mu_{X,z} c_{X,z} \mathbf{E}) + \nabla \cdot (D_{X,z} \nabla c_{X,z}) + R_{X,z}(c_Y)$	Concentrations in terms of $g_{X,z}$ , finite dilution $pK_a$ , and finite dilution mobility $\mu_{X,z}^0$	Davies equation for $pK_a$ , Pitts for mobilities. See also equation (13).
Mass transport	Concentrations in fluxes, activities in source terms $\frac{Dc_{X,z}}{Dt} = \nabla \cdot (\mu_{X,z} c_{X,z} \mathbf{E}) + \nabla \cdot (D_{X,z} \nabla c_{X,z}) + R_{X,z}(\gamma_Y c_Y)$	Concentrations in fluxes, activities in source terms	Davies equation for $pK_a$ , Pitts for mobilities. See also equation (13).

<sup>a</sup> Note that there are exceptions. For example enzymatic affinity constants are defined in terms of concentrations, but not derived from the law of mass action.<sup>32, b</sup> This does not only involve electrolytes but also neutral species. The ideal dilute approximation is a hypothetical state where reactions are independent of ionic strength and diffusion limited.

These principles and formulations are applicable to more general formulations including generalized mass transport calculations.<sup>27</sup>

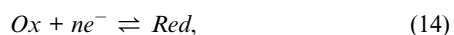
We note that diffusion coefficients also depend on ionic strength. At finite ionic strength, the Nernst-Einstein equation<sup>28</sup> breaks down. For example, the effective diffusivity of potassium chloride reportedly decreases from approximately  $2.0 \times 10^{-9} \text{ m}^2 \text{ s}^{-1}$  at infinite dilution to  $1.8 \times 10^{-9} \text{ m}^2 \text{ s}^{-1}$  at 100 mM, and increases again at larger concentrations (e.g.  $2.0 \times 10^{-9} \text{ m}^2 \text{ s}^{-1}$  at 2 M).<sup>8</sup> Harned and Nuttall<sup>29</sup> showed good agreement between their measurements and theoretical predictions of diffusion coefficients by the Onsager and Fuoss theory. For detailed treatment of diffusion coefficients in non-dilute solutions, refer to Robinson and Stokes.<sup>8</sup>

## Electrochemical effects

In this section we summarize electrolysis reactions that occur at primary electrodes which drive current and flow in electrokinetic systems. We describe a general model of potential loss applicable to electrokinetic systems, and develop detailed models of electrochemical and Ohmic potential losses for common on-chip capillary electrophoresis systems. We focus on the typical case of direct current (DC) electrokinetic microsystems with aqueous electrolytes wherein microchannel networks are connected to end-channel reservoirs containing electrochemically stable electrodes (often platinum).

### Reduction–oxidation reactions

Acid–base equilibrium is a subset of a more general concept of reduction–oxidation (redox). A redox reaction involves the transfer of  $n$  electrons,  $e^-$ , between species and follows the general mechanism:



where *Ox* is the oxidant (electron acceptor) and *Red* is the reductant (electron donor). The forward reaction is termed a reduction reaction, and the reverse an oxidation reaction. For example, in acid–base equilibrium, the acid is an oxidant and its conjugate base a reductant. The equilibrium between oxidant and reductant is characterized by a redox potential, measuring the affinity of the species to electrons. In the case of electrochemical cells, the redox potential is called the standard electrode potential.

Redox reactions are at the basis of electrochemical phenomena. The transfer of electrical current from a source to a solution involves exchange of electrons at the interface between the polarizable surface (the electrode) and the liquid. This transfer generates the Faradaic current.

### Electrolysis in electrokinetic systems

Consider a power source supplying a steady current to a microfluidic device, through two electrodes immersed in the electrolyte. Redox reactions occurring at electrodes sustain current: an oxidation reaction occurs at the anode, and a reduction at the cathode. The net reaction is the sum of the “half reactions” of oxidation and reduction, referred to as electrolysis. For EK systems, water electrolysis is most often the dominant electrolytic

**Table 2** Electrode reactions for water electrolysis, the OER occurs at the anode, and the HER at the cathode. The overall oxygen and hydrogen evolution reactions depend on solution pH<sup>38,39</sup>

	Acidic Solution	Alkaline Solution
Anode (OER)	$2\text{H}_2\text{O} \rightarrow 4\text{H}^+ + 4e^- + \text{O}_2$	$4\text{OH}^- \rightarrow 4e^- + \text{O}_2 + 2\text{H}_2\text{O}$
Cathode (HER)	$2\text{H}^+ + 2e^- \rightarrow \text{H}_2$	$2\text{H}_2\text{O} + 2e^- \rightarrow \text{H}_2 + 2\text{OH}^-$

reaction.<sup>33–37</sup> Water electrolysis is often referred to as the oxygen evolution reaction (OER) at the anode, and the hydrogen evolution reaction (HER) at the cathode.

The overall form of the OER and HER depends on the electrolyte pH, as summarized in Table 2. For the HER, the negative surface charge of the cathode removes protons from solution.<sup>38,39</sup> In acidic solutions, hydronium has relatively high concentration. As a consequence, it is the dominant proton donor (i.e. electron acceptor). In alkaline solutions, hydronium has lower concentration, and water becomes the dominant electron acceptor. In the OER, the anode accepts electrons from hydroxide in alkaline solution or from water in acidic solution. The effect is an increase in pH at the cathode reservoir and a decrease at the anode reservoir.<sup>33–37,40–44</sup> Table 2 shows that supplying low-frequency\*\* or DC currents to electrokinetic systems result in several, often undesirable phenomena. These include the generation or consumption of hydronium or hydroxide ions at the driving electrodes, which result in spatial and temporal variations in background electrolyte pH and conductivity.<sup>33–37,40–44</sup> In addition, the generation of hydrogen and oxygen gas bubbles at driving electrodes can complicate the “chip to world” connection and can block or be entrained into a channel.<sup>37,41,45</sup> Bubble management and control of pH changes are key to optimization and repeatability of EK experiments.

### Electrolysis pH changes: Transport and mitigation strategies

As we mentioned above, in electrokinetic systems the anode reactions tend to decrease local pH, while the cathode reactions raise local pH. Transport of regions of perturbed pH from near the electrode surface, into the reservoir volume and the channels is a complex problem involving electrode reactions, multispecies diffusion and electromigration, and fluid flow into and out of the reservoir. Visualizations of the spatiotemporal development of such pH fields was performed by Macka *et al.*<sup>36</sup> Their setup included 0.5 mm diameter platinum wires immersed into buffered and unbuffered chromate with xylenol blue dye as a pH indicator, and acetate buffer with bromocresol green dye. Their reservoirs were 2 mm deep (along the optical axis of their imaging) and 10 by 40 mm in the image plane. Their visualizations show that, for low viscosity electrolytes, convective fluid transport greatly contributes to the spatiotemporal development

\*\* A simplified model of the electrode/electrolyte interface is that of a capacitor and resistor in parallel, where the capacitor models electric double layer charging and resistor charge transfer across the interface.<sup>47</sup> At high enough frequencies, the current supplied to the electrode will serve mostly to charge the double layer, and negligible charge is allowed to cross the interface (negligible Faradaic current) before polarity reverses.<sup>47</sup>

of the pH field in the reservoir. In any case, the general problem is quite complex and can involve thermal convection, bubble nucleation and growth phenomena, bubble detachment and bubble-driven flow, and coupled convective-diffusion of pH fields.

There are several strategies for mitigation of electrokinetic buffer depletion. These include appropriate use of buffers to ensure pH stability (*cf.* Part I); frequent buffer replenishments,<sup>33,34,42</sup> the use of low conductivity (*e.g.*, zwitterionic) buffers to reduce current,<sup>37,40,44</sup> large electrode-to-channel distances to confine reaction zones,<sup>36,37</sup> and increasing reservoir size<sup>37</sup> to both confine reaction zones and improve total buffering capacity. However, one clear advantage of on-chip CE type applications over traditional systems is their ability to deal with small sample volumes.<sup>37</sup> Therefore increasing reservoir size and electrode-to-channel distances is often counterproductive. Predictive models for transient reservoir pH have been presented by Bello<sup>33</sup> and Corstjens *et al.*,<sup>34</sup> and these provide guidelines for the required frequency of buffer replenishment. Below, we present a model allowing estimation of pH changes in a typical microfluidic EK experiment.

### pH changes during an electrokinetic experiment weak electrolyte buffer

Consumption and production of hydronium and hydroxide ions in the reservoirs (*cf.* Table 2) can affect electrolyte chemistry and impact the performance of the entire system. We here model and discuss quantitatively the effects of concentration changes induced by electrode reactions.

We present an illustrative model which accounts for the effect of electrode reactions on a system composed of a single channel connecting two reservoirs as shown in Fig. 2. The buffer system is a weak base B (*e.g.*, Tris base), titrated with a strong acid HA (*e.g.*, hydrochloric acid HCl) to a desired pH. We will later present results of the analogous problem of a weak acid titrated

with a strong base. We perform a control volume analysis with the following assumptions: (i) electrode reactions are solely water electrolysis, (ii) electroneutrality applies everywhere in the system, (iii) hydronium and hydroxide ions do not carry current, (iv) the solution is dilute (so that  $\mu_{X,z}^{\infty} = \mu_{X,z}^{\infty}$  and  $pK = pK_I = 0$ ), (v) advective current is negligible (in particular electroosmotic flow is negligible), and (vi) the reservoirs are “well stirred” so the concentrations are uniform within each reservoir. Although simplified, this example problem is sufficient to summarize and review relevant dynamics of these problems and point out key parameters. As discussed and visualized by Macka *et al.* pH changes originate at the electrode surface and are transported by diffusion and advection (*e.g.*, due to thermal convection and bulk flow from the reservoir into the channel). Assuming negligible thermal convection (*i.e.*, sufficiently small reservoirs), we can assume pH perturbations originate at the electrode and transport outward. In such cases, we hypothesize that a well-stirred reservoir approximation will overpredict the effects of electrode reactions on the channel flow. We therefore take this well-stirred assumption as a conservative estimate in estimating experiment durations and reservoir volumes required to avoid pH changes in a connecting microchannel(s).

We consider a constant voltage experiment, but the model can be readily modified for (the simpler case of) constant current conditions. The potential drop between anode and cathode  $V_{app}$  generates an electric field of magnitude  $V_{app}/L$  in the channel. The current  $i$  sets the rate of creation of hydronium ions at the anode and hydroxide ions at the cathode. As in most experimental studies, we assume constant voltage, and so the current adjusts to the electrolyte conductivity in the channel,  $\sigma^{ch}$ , where the superscript *ch* designates the channel. For a channel of cross sectional area  $S$ , the current is simply  $i = V_{app}(\sigma^{ch}S/L)$ . Applying electroneutrality inside the channel ( $c_{A,-1}^{ch} = c_{B,+1}^{ch}$  under “moderate pH” conditions<sup>7</sup>), and under the assumption that only buffer species carry current (*i.e.*, “safe pH”), the conductivity simplifies to  $\sigma^{ch} = Fc_{A,-1}^{ch}(\mu_{B,+1}^{\infty} - \mu_{A,-1}^{\infty})$ . Recall that  $\mu_{X,z}^{\infty}$  is the fully ionized mobility of X in valence state  $z$ .

The Faradaic current induces migration of the anion  $A^-$  from the cathode to the anode. The fluxes of  $A^-$  into the anode reservoir and out of the cathode reservoir are respectively  $J_{A,-}^a = -\mu_{A,-1}^{\infty}c_{A,-1}^{ch}(V_{app}S/L)$  and  $J_{A,-}^c = \mu_{A,-1}^{\infty}c_{A,-1}^{ch}(V_{app}S/L)$ , where the superscripts *a* and *c* designate respectively anode and cathode reservoirs. Current flow therefore depletes the cathode reservoir of buffer anions (replacing them with hydroxide ions). We can write the conservation of A in the cathode reservoir:

$$\frac{dc_{A,-1}^c}{dt} = c_{A,-1}^c \left( \frac{\mu_{A,-1}^{\infty} V_{app} S}{\Upsilon L} \right), \quad (15)$$

where  $\Upsilon$  is the reservoir volume (equal for anode and cathode). This first order ordinary differential equation yields an exponential decay of the concentration of A from its initial value  $c_{A,-1}^0$  with characteristic time scale  $\tau = -\Upsilon L / (i(\mu_{A,-1}^{\infty} V_{app} S))$  ( $\mu_{A,-1}^{\infty} < 0$  so that  $\tau > 0$ ) in the cathode reservoir:

$$c_{A,-1}^c(t) = c_{A,-1}^0 \exp(-t/\tau). \quad (16)$$

Similarly, the rate of change of anion concentration at the anode is

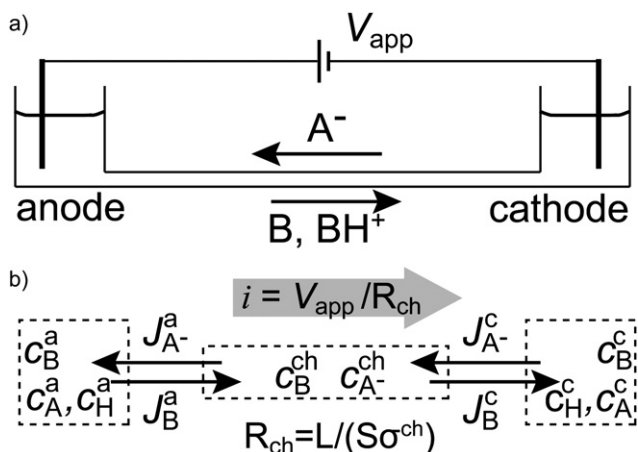


**Fig. 2** Schematic of an electrokinetic experiment where the electrolyte is a solution of a weak base titrated with a strong acid. The anion  $A^-$  migrates towards the anode. The cation  $BH^+$  migrates towards the cathode with an effective mobility determined by its ionization state (and local pH). The anode and cathode respectively lower and raise local pH over time.

$$\frac{dc_{A,-1}^a}{dt} = -c_{A,-1}^{ch} \left( \frac{\mu_{A,-1}^\infty V_{app} S}{\gamma L} \right). \quad (17)$$

The conservation of  $A^-$  in the channel  $J_{A,-}^c + J_{A,-}^a = 0$  yields  $c_{A,-1}^c = c_{A,-1}^{ch}$ , so that (17) becomes:

$$\frac{dc_{A,-1}^a}{dt} = \frac{c_{A,-1}^0}{\tau} \exp(-t/\tau), \quad (18)$$

which after integration yields:

$$c_{A,-1}^a(t) = c_{A,-1}^0 [2 - \exp(-t/\tau)]. \quad (19)$$

Using the expression of conductivity, we can derive the expression of current as a function of time:

$$i = \frac{F\gamma c_{A,-1}^0}{\tau} (1-f)^{-1} \exp(-t/\tau), \quad (20)$$

where  $f = \mu_{B,+1}^\infty / (\mu_{B,+1}^\infty - \mu_{A,-1}^\infty)$  is the transport number, measuring the contribution of the cation to current conduction. Similarly, the flux of B out of the anode is:

$$J_B^a = -\mu_B^a c_B^a (V_{app} S/L) = -\mu_{B,+1}^\infty c_{B,+1}^a (V_{app} S/L). \quad (21)$$

Note  $c_B^a$  and  $\mu_B^a$  are respectively the total concentration and the effective mobility of species B at the anode,<sup>7</sup> and these describe total outflow of B and  $BH^+$ .  $c_{B,+1}^a$  and  $\mu_{B,+1}^\infty$  are the respective concentration and mobility of (specifically) the cation state  $BH^+$ . Applying electroneutrality to the anode reservoir, we have  $J_B^a = -\mu_{B,+1}^\infty c_{A,-1}^a (V_{app} S/L)$ . In the anode, electromigration depletes the buffer of species B, replacing it with protons. In the same manner as the case of the anode and equation (15), we can derive the rate of change of weak base in the anode reservoir:

$$\frac{dc_B^a}{dt} = \frac{J_B^a}{\gamma} = \frac{c_{A,-1}^a}{\tau} \frac{\mu_{B,+1}^\infty}{\mu_{A,-1}^\infty}. \quad (22)$$

We recognize that  $\mu_{B,+1}^\infty / \mu_{A,-1}^\infty = f/(f-1)$ , so that:

$$c_B^a = c_B^0 + c_{A,-1}^a f (f-1)^{-1} \left( 2 \frac{t}{\tau} + \exp(-t/\tau) - 1 \right). \quad (23)$$

Similarly, at the cathode well:

$$c_B^c = c_B^0 + c_{A,-1}^c f (1-f)^{-1} (1 - \exp(-t/\tau)). \quad (24)$$

We note that from the initial equilibrium  $c_{A,-1}^0 = c_B^0 (1 + 10^{\text{pH}^0 - \text{p}K_a})^{-1}$  where the buffer is initially titrated to  $\text{pH}^0$ . We then find the pH in the anode reservoir from the Henderson-Hasselbalch equation (see eq. (8) of Part I):<sup>7</sup>

$$\begin{aligned} \text{pH}^a &= \text{p}K_a + \log_{10} \left[ \frac{c_B^a - c_{A,-1}^a}{c_{A,-1}^a} \right] \\ &= \text{p}K_a + \log_{10} \left[ \frac{10^{\text{pH}^0 - \text{p}K_a} + f(f-1)^{-1} (f^{-1} + 2t/\tau + \exp(-t/\tau))}{2 - \exp(-t/\tau)} - 1 \right]. \end{aligned} \quad (25)$$

We can derive the pH variation at the cathode in the same manner:

$$\begin{aligned} \text{pH}^c &= \text{p}K_a + \log_{10} \left[ \frac{c_B^c - c_{A,-1}^c}{c_{A,-1}^c} \right] \\ &= \text{p}K_a + \log_{10} \left[ \left( 10^{\text{pH}^0 - \text{p}K_a} + (1-f)^{-1} \right) \exp(t/\tau) - (1-f)^{-1} \right]. \end{aligned} \quad (26)$$

We note from equations (25) and (26) that the variations of pH at the cathode or the anode do not depend on initial buffer concentration. That is, at constant applied voltage, the pH changes due to electrode reactions are independent of buffer concentration. This result is intuitive since both buffer capacity

**Table 4** Summary of pH changes in the anode and cathode for a weak base buffer strong acid titrant, and a weak acid buffer, strong base titrant in the limits where  $t \ll \tau$  and pH is initially close from  $\text{p}K_a$ . Each equation is an expression of  $\Delta\text{pH} = \text{pH} - \text{pH}^0$ . The parameter  $\alpha = 10^{\text{pH}^0 - \text{p}K_a}$  is an indicator of buffer strength

	Anode	Cathode
Weak base buffer, strong acid titrant	$-\frac{f(\alpha-1) + \alpha + 1}{\alpha(1-f)} \frac{t}{\tau}$	$\frac{\alpha + 1 - \alpha f}{\alpha(1-f)} \frac{t}{\tau}$
Weak acid buffer, strong base titrant	$-\frac{\alpha(1-f)}{f} \frac{t}{\tau}$	$\frac{\alpha + f}{f} \frac{t}{\tau}$

**Table 3** Summary of pH changes in the anode and cathode for a weak base buffer titrated with a strong acid, and a weak acid buffer titrated with a strong base. Each equation is an expression of  $\text{pH} - \text{p}K_a$

	Anode	Cathode
Weak base buffer, strong acid titrant	$\log_{10} \left\{ \frac{10^{\text{pH}^0 - \text{p}K_a} + f(f-1)^{-1} (f^{-1} + 2t/\tau + \exp(-t/\tau))}{2 - \exp(-t/\tau)} - 1 \right\}$	$\log_{10} \{ (10^{\text{pH}^0 - \text{p}K_a} + (1-f)^{-1} \exp(t/\tau) - (1-f)^{-1}) \}$
Weak acid buffer, strong base titrant	$-\log_{10} \{ 10^{-\text{pH}^0 + \text{p}K} + (f^{-1} - 1) [\exp(t/\tau) - 1] \}$	$-\log_{10} \left\{ \frac{10^{-\text{pH}^0 + \text{p}K} + f^{-1} - (f^{-1} - 1) [2t/\tau + \exp(-t/\tau)]}{2 - \exp(-t/\tau)} - 1 \right\}$

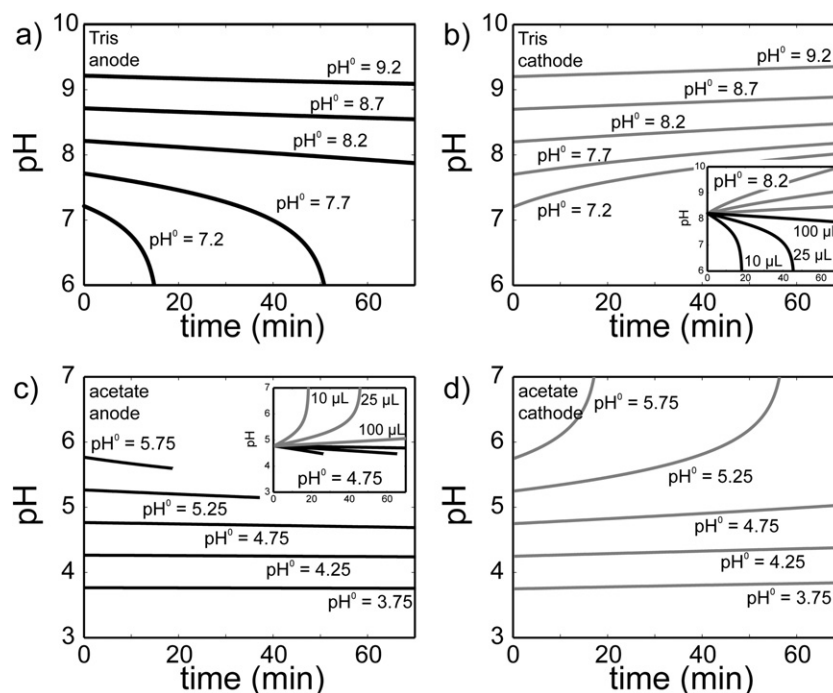


**Fig. 3** Effect of electrode reaction on anode pH and cathode pH for Tris and acetate buffers titrated with respectively hydrochloric acid and sodium hydroxide. (a) and (b): pH variation for 10 mM Tris initially titrated with hydrochloric acid to  $\text{pH}^0$ , which is varied from  $\text{p}K_a - 1$  to  $\text{p}K_a + 1$ . We consider 2.5 kV applied to a 5 cm long, 50  $\mu\text{m}$  wide (20  $\mu\text{m}$  deep) channel. (a) pH at the 100  $\mu\text{L}$  anode reservoir. If initial pH is below  $\text{p}K_a$ , the anode pH drops dramatically, as the anode generates  $\text{H}^+$ . (b) pH at the 100  $\mu\text{L}$  cathode reservoir. The pH change is slow as the cathode reservoir fills with weak base. Inset: anode (black solid lines) and cathode (grey solid lines) pH for 10  $\mu\text{L}$ , 25  $\mu\text{L}$  and 100  $\mu\text{L}$  reservoirs and  $\text{pH}^0 = \text{p}K_a$ . (c) and (d): pH variation for 10 mM acetate buffer (titrated with sodium hydroxide) in otherwise the same conditions as the previous case. (c) pH at the 100  $\mu\text{L}$  anode reservoir. The pH change is slow as the anode reservoir fills with weak acid. Inset: anode (black solid lines) and cathode (grey solid lines) pH for 10  $\mu\text{L}$ , 25  $\mu\text{L}$  and 100  $\mu\text{L}$  reservoirs and  $\text{pH}^0 = \text{p}K_a$ . (d) pH at the 100  $\mu\text{L}$  cathode reservoir. If initial pH is above  $\text{p}K_a$ , the cathode pH increase dramatically, as the cathode generates  $\text{OH}^-$ .

and current are directly proportional to buffer concentration. The two important parameters are: (i) the time scale  $\tau = -Y L / (\mu_{\text{X},-1} V_{\text{app}} S)$ ; and (ii) the initial buffer pH. We summarize the closed form solutions for pH at the anode and cathode of a weak base buffer system (derived above) and a weak acid buffer system (derivation not shown) in Table 3.

For convenience and quick estimates, we summarize in Table 4 the same relations but in the limit where the experiment time is much smaller than the characteristic time scale,  $\tau$ .  $\tau$  ranges between 1 and 100 min for typical EK systems (see examples below). The parameters in Table 4 can be interpreted as a fairly general set of non-dimensional parameters describing the importance of pH changes due to electrolysis in buffer reservoirs. These expressions are simplified and yet capture the effects of proper titration (via the parameter  $\alpha = 10^{\text{pH}^0 - \text{p}K_a}$ ), the effect of ion mobilities (via  $f$ ), and the relative magnitude of the experiment time to the characteristic time constant. The latter depends on buffer concentration, reservoir volume, and applied voltage. Absolute values of the parameter  $t/\tau$  smaller than  $\sim 0.05$  are a good indication that pH changes should be negligible.

Fig. 3 shows examples of pH changes in 100  $\mu\text{L}$  (each) anode and cathode reservoirs during an electrophoresis type experiment for two buffer systems: 10 mM Tris ( $\text{p}K_a = 8.2$ ) titrated with HCl or 10 mM acetic acid ( $\text{p}K_a = 4.8$ ) titrated with NaOH. pH drops dramatically in the anode reservoir for the Tris buffer system for the cases where initial pH is below its  $\text{p}K_a$ . Conversely, we see pH

increases dramatically in the cathode reservoir for the acetate buffer system for cases where the initial pH is higher than its  $\text{p}K_a$ . More generally, pH changes dramatically in reservoirs towards which the titrant ion migrates; and pH changes relatively slowly in the other reservoir. Further, we see that rapid variations in the anode and cathode can, in all cases, be limited by titrating the buffer to respectively higher and lower pH. For example, Fig. 3a shows that if Tris is titrated slightly above its  $\text{p}K_a$ , it buffers more efficiently at the anode (while acetate buffer titrated with slightly below its  $\text{p}K_a$  buffers more efficiently at the cathode, as in Fig. 3d). In this way, anode and cathode reservoir chemistry can be slightly adjusted to “anticipate” the effects of the anode and cathode reactions.<sup>††</sup> The insets show the expected result that larger reservoirs are more robust to pH changes in both acid and basic buffer systems. Lastly, we note that pH changes are independent of buffer strength only at constant voltage, as it is only dependent on the amount of charges (Coulombs) transferred to the liquid (and both charge transfer and current in and out of the reservoirs is proportional to buffer strength). We note, however,

<sup>††</sup> One strategy in systems with significant electroosmotic (or other bulk) flow may therefore be to slightly adjust buffer pH to “anticipate” the change in the flow inlet reservoir. For example, for a Tris hydrochloride buffer in glass channels and pure electroosmotic flow (no pressure-driven flow), you might titrate the buffer to favor the anticipated creation of acid in the anode reservoir. Accordingly, you might titrate to  $\sim 0.5$  pH units above the Tris  $\text{p}K_a$ .

that buffering strength is a critical parameter in constant current experiments.<sup>34</sup>

### Back-of-the-envelope calculation for importance of pH change due to electrolysis

In most electrokinetic applications, we are dealing with moderate pH conditions and also the conductance between two end-channel electrodes is approximately constant. For such cases, the time scale for pH change due electrolysis current  $i$  in a reservoir volume  $Y$  can be expressed as  $\tau = Y\sigma/(iz\chi\mu_{\text{X}}^{\infty})$  (since  $i = \sigma(V_{\text{app}}/L)S$ ) for both the anode and cathode reservoirs. Here,  $\mu_{\text{X}}^{\infty}$  is the mobility of the titrant (*i.e.*, strong acid or base). This time scale can be used to provide a rough, order-of-magnitude estimate for the time before we should expect a significant change in pH. For example, consider typical values of  $Y = 5 \mu\text{l}$ ,  $i = 20 \mu\text{A}$ , and  $\sigma = 0.5 \text{ mS/cm}$  (consistent with 10 mM Tris titrated with HCl to pH = 8.2, 500 V  $\text{cm}^{-1}$  field in a D-shaped channel 50  $\mu\text{m}$  wide, 15  $\mu\text{m}$  deep channel). For a typical buffer such as Tris titrated with HCl,  $\mu_{\text{X}}^{\infty} = \mu_{\text{Cl}^{-}}^{\infty} = -79.1 \times 10^{-9} \text{ m}^2 \text{ V}^{-1} \text{ s}^{-1}$ . This yields  $\tau \approx 3 \text{ min}$ . Provided the electrode is placed in the reservoir away from the channel entrance, experiments with durations significantly shorter than this (less than 20 s or shorter) should not suffer from significant pH change. This example is easily scalable to other systems; so increasing the reservoir to 50  $\mu\text{l}$  yields  $\tau = 30 \text{ min}$ . The latter suggests steady pH operation for order 3 min.

Our results are in qualitative agreement with the work of Corstjens *et al.*<sup>34</sup> who studied the effect of electrolysis in constant current CE experiments at finite dilution. Bello<sup>33</sup> studied a more complex buffer system and modeled electrolysis effects in constant voltage CE experiments with no assumption on pH (*i.e.*, hydronium and hydroxide can have a significant concentration). The parameters from both studies are perhaps more suitable to classical CE systems (*i.e.*, channels longer than 10 cm, and reservoir volumes larger than 0.5 mL) but are qualitatively similar to a microfluidic electrokinetic case.

We derived a simple expression for the pH changes in well-stirred reservoirs. We note that more general treatments of this problem can be very complex. For example, the physics involved in the ionic transport within the reservoirs is in general a complex, multi-species reaction equilibrium transport problem. Possible additional phenomena include thermally driven buoyancy fluid motion near the electrode;<sup>36</sup> surface tension effects due to the change of contact angle between fluid surface and electrode;<sup>46</sup> flow induced by bubble nucleation and growth; flow induced by bubble detachment and bubble motion toward the top of the reservoir; flow in reservoir induced by electroosmotic flows; and pressure gradients induced by changes in reservoir volume. The visualizations of Macka *et al.*<sup>36</sup> confirm that the spatio-temporal distribution of pH in an electrophoresis system reservoir is indeed a complex process.

### Electrolysis bubbles

Water electrolysis generates oxygen gas at the anode and hydrogen gas at the cathode (see Table 2). More precisely, hydrogen and oxygen atoms adsorbed onto the cathode and anode electrode surface respectively, react to form gaseous  $\text{O}_2$  or  $\text{H}_2$ .<sup>47</sup> Electrolytic gas bubbles form at nucleation sites on the

electrode surface or supersaturation regions in the electrolyte near the electrode interface.<sup>48</sup> The growth of adsorbed bubbles shields the electrode surface, decreasing the electrode real surface area,  $S_r$ , and dropping the system limiting current.<sup>48,49</sup> Bubbles may eventually separate from the electrode surface and leave the reservoir driven by buoyancy or may in some cases be advected into the channel, causing blockage.<sup>37,41</sup> Adsorbed or detached bubbles in the channel or reservoir increase interelectrode resistance,<sup>49</sup> resulting in a current drop for potentiostatic operation. Note that, for the same current, the rate of hydrogen production at the cathode is twice that one of oxygen at the anode.

Several mitigation strategies applicable to on-chip capillary electrophoresis can prevent bubble entrainment into the channel or bubble generation entirely. Displacing electrodes from the channel entrance may be effective in preventing bubbles from entering the channel.<sup>37</sup> Several groups have used ion exchange membranes such as Nafion to prevent bubble advection into the channel.<sup>50,51</sup> Moini *et al.*<sup>52</sup> demonstrated that introducing hydroquinone (HQ) into the buffer allows for HQ oxidation to replace water oxidation at the anode, resulting in the formation water soluble p-benzonquinone. Recently, Kohlheyer *et al.*<sup>53</sup> used quinhydrone to prevent both oxygen and hydrogen bubble formation, which at their experimental conditions was effective up to approximately 40  $\mu\text{A}$ . Another possible method is operation in a degassed electrolyte which allows dissolution of gases produced at the electrode.<sup>54</sup> Lastly, palladium electrodes have been shown to absorb some hydrogen, and thus may in some cases help mitigate hydrogen gas formation at the cathode.<sup>55</sup>

### Potential losses in CE systems

Consider a simple electrokinetic system consisting of a micro-channel connecting two reservoirs each containing an electrode. The potential applied to the electrodes of this system does not entirely drop across the microchannel. Instead, finite potential differences exist between the electrode surface and channel entrance. This is due to (i) a potential difference across the electrode-electrolyte interface which drives electrochemical reactions occurring at electrode surfaces, and (ii) a potential drop between the electrode surface and channel entrance associated with current through the reservoirs (an Ohmic loss). Many on-chip electrophoresis systems use high voltages (100 V to 10 kV) and so are largely insensitive to the typically small voltage losses associated with electrochemical reactions (as will be shown in Fig. 6). However, these losses can become important in systems which use relatively low voltage (*e.g.*, smaller than 20 V). Examples of these include low voltage electrophoretic separations,<sup>56-59</sup> and low voltage electroosmotic pumping.<sup>60,61</sup> In contrast, Ohmic loss in the reservoirs can form a significant portion of applied potential for both low and high voltage systems (as will be shown in Fig. 5). Accounting for reservoir potential drop is particularly important for analyzing strategies which involve changing reservoir geometry or electrode placement to confine electrode reactions.<sup>36</sup>

The voltage applied to a typical single channel device can be expressed in terms of the potential drop across the channel,  $V_c$ , and several sources of potential loss as follows:

$$V_{\text{app}} = V_c + E_{\text{eq}} + \eta_a + \eta_c + V_{\text{res,ar}} + V_{\text{res,cr}} \quad (27)$$

$E_{eq}$  is the equilibrium potential of redox reactions, and can be computed from the Nernst equation.<sup>62</sup> The Nernst equation relates the standard electrode potential with the effects of non-standard pressure, temperature, and solute activities. Bard<sup>62</sup> (Appendix C) and Bockris<sup>47</sup> (Chapter 7, p. 1352) list standard electrode potentials in aqueous solutions for a variety of reduction reactions. A Faradaic current, or the driving current required for typical electrokinetic experiments, is theoretically possible only for  $V_{app} > E_{eq}$ . The overpotential,  $\eta$ , represents the potential required to drive the rate limiting step of the electrode reaction at the desired Faradaic current.<sup>47</sup>  $V_{res}$  is the Ohmic potential drop maintained between the electrode surface and the channel entrance. The second subscripts in equation (27) refer to the anode (*a*) cathode (*c*), anode reservoir (*ar*), and cathode reservoir (*cr*), respectively.

We leverage the Tafel equation for overpotential and Ohm's law for  $V_c$  and  $V_{res}$  to express potential drops in our system as follows:

$$V_{app}(t) = \int_0^L \frac{I}{\sigma(x,t)S} dx + E_{eq} + b_a \ln \left( \frac{I}{j_{o,a} S_{r,a}} \right) + \dots \quad (28)$$

$$\frac{I}{\sigma_{ar}(t) S_{eff}} + \frac{I}{\sigma_{cr}(t) S_{eff}}$$

$\sigma_{ar}$ ,  $\sigma_{cr}$ , and  $\sigma$  are respectively the conductivity in the anode reservoir, cathode reservoir and channel. Our major assumptions for the expression of  $V_c$  include 1-D conductivity gradients in the microchannel, and negligible contribution of bulk fluid motion to ionic current (*i.e.*, negligible advective current).<sup>47</sup> The latter assumption allows for modeling  $V_c$  using Ohm's law. In modeling  $V_{res}$ , we have assumed spatially uniform conductivity within each reservoir and reservoirs with identical geometry. Note that reservoir conductivity may change in time due to addition or removal of charged species by the electrochemical reactions summarized in Table 2.  $S$  is the channel cross sectional area, and  $S_{eff}$  and  $L_{eff}$  are effective parameters which represent the cross sectional area and path length of the ionic current in the reservoir. These parameters account for three-dimensional reservoir geometry and current distribution, and will be discussed further below.

For the Tafel equation, the parameter  $b$  is a function of temperature and a symmetry factor, and dividing  $b$  by the factor 2.3 yields a parameter known as the Tafel slope.<sup>47</sup> Tafel slope has been reported as roughly 120 mV/dec (*i.e.* mV per "decade" slope in a semilog plot) for the HER and OER.<sup>‡‡</sup><sup>47,63,64</sup> The exchange current density,  $j_o$ , physically represents the bi-directional current at equilibrium (at  $V_{app} \leq E_{eq}$ ), and is often used to describe the kinetics of the chemical reaction at the electrode.<sup>47</sup> With platinum electrodes, the exchange current density of the HER and OER are of the order  $10^{-4}$  A cm<sup>-2</sup> and  $10^{-9}$  A cm<sup>-2</sup> respectively, for both acidic and basic conditions.<sup>65</sup> As a result, for water electrolysis the anode exchange current density,  $j_{o,a}$ , is several orders of magnitude smaller than  $j_{o,c}$ , and thus  $\eta_a \gg \eta_c$ . We have thus neglected  $\eta_c$  in equation (28).  $S_r$  is the real electrode

surface area, meaning the surface area on which electron transfer occurs. For platinum wire electrodes,  $S_r$  differs from the simple wire geometric surface area,  $S_{geom}$ , due to surface roughness.<sup>62,66</sup> Real surface area of a platinum wire electrode can be estimated by a variety of in-situ or ex-situ experimental methods, which are extensively described and evaluated by Trasatti *et al.*<sup>66</sup>

We invoke the Tafel equation by assuming high overpotential (greater than approximately 100 mV), and that concentration of OER and HER reactants at their respective electrode surfaces is within 10% of the reactant concentration in the bulk electrolyte.<sup>62</sup> The high overpotential assumption is reasonable for the OER reaction at currents characteristic of electrokinetic experiments (order  $\mu$ A currents and above), due to the low OER exchange current density (see Fig. 6). For simplicity, we additionally assume  $j_{o,a}$  and  $b_a$  are not functions of applied potential.<sup>47</sup> Despite further complexities associated with precise modeling of electrode reactions (*e.g.*, including the effect of pH changes in reservoirs on HER and OER overpotentials<sup>39</sup>), the model presented here allows for basic parametric studies and insights into the sources of these potential losses.

### Estimates of Ohmic voltage drop in typical reservoirs

We here estimate the relative importance of the Ohmic potential drop in electrokinetic reservoirs for typical microchannel geometries. We consider a cylindrical reservoir with a diameter-to-liquid-height ratio of unity and an approximately cylindrical microchannel connected to the reservoir at the bottom right, as in Fig. 4. The electrode is a thin, vertical, and cylindrical wire placed along the wall of the reservoir diametrically opposed to the channel as shown. We recommend the latter placement in experiments as: (i). the wire is kept well away from the channel entrance to mitigate the effects of pH changes and bubbles generated by the electrode; and (ii). placing the tip of the wire at the bottom of the reservoir is easier to reproduce (*vs.* suspending the wire part way down the reservoir). Assuming approximately uniform conductivity within each reservoir, the geometric parameter  $L_{eff}/S_{eff}$  can be calculated by use of a numerical solution to the conservation of current relation assuming uniform (locally, for each domain) conductivity, which yields:

$$\nabla^2 \phi = 0, \quad (29)$$

where  $\phi$  is local potential. As shown in Fig. 4, we modeled potential drop in a reservoir connected to a 0.5 mm long microchannel section. The channel length is significantly longer than the length yielding approximately uniform and parallel electric field in the channel (see Fig. 4). We rounded the edges of the transition between reservoir and channel using fillets with 10  $\mu$ m radii of curvature. The boundary conditions are: specified potential at the electrode surface,  $V_{elec}$ ; specified potential surface 0.5 mm into the small channel; and zero normal current at all other surfaces. The three-dimensional potential field was solved with a commercially available finite element simulation software (Comsol Multiphysics 3.3a, Burlington, USA). Solutions were obtained using over  $8 \times 10^4$  tetrahedral mesh elements; were mesh size independent; and converged with over 8 orders of magnitude decrease in the residual. To estimate the

‡‡ We note that reported Tafel slope varies between about 50 and 200 mV/dec for a range of electrode materials, electrolyte chemistry, and pH.<sup>47,63,64</sup> We report here 120 mV/dec only as a typical value.

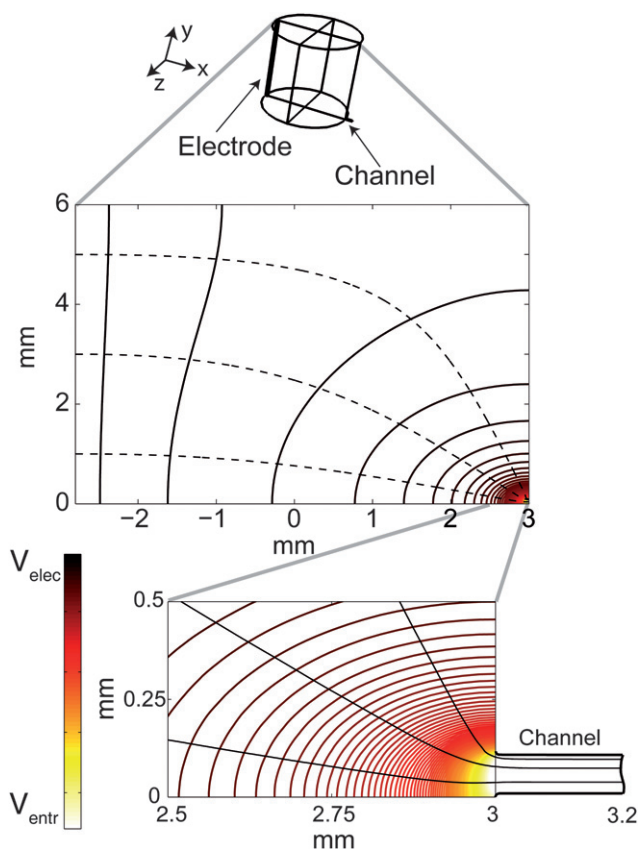


**Fig. 4** Model geometry and results showing evenly-spaced equipotential lines and dashed current lines in the  $x$ - $y$  midplane of a  $D = 6$  mm (height and diameter) reservoir. Detail view shows the near-channel region of the reservoir, and current lines are shown as they continue into the  $d = 100$   $\mu\text{m}$  channel. The potential drop in the reservoir is dominated by the drop in the near-channel region (where stream lines crowd). This effect explains insensitivity of ionic resistance to reservoir size, and allows us to conclude that for this typical configuration (*i.e.*, vertical wire touching bottom of well) and geometries ( $D = 2$ – $10$  mm,  $d = 20$ – $100$   $\mu\text{m}$ ), potential loss between the electrode surface and channel entrance is largely independent of  $D$ . Instead, reservoir potential loss is highly sensitive to microchannel diameter,  $d$ . Also note that current lines, and thus electric field lines, become parallel after approximately a distance  $d$  into the channel.

geometric parameter  $L_{\text{eff}}/S_{\text{eff}}$  associated with the reservoir, we first compute the area-average potential at the channel inlet,  $V_{\text{entr}}$ , from model results; and then define the potential loss in this reservoir,  $V_{\text{res}}$ , as follows:

$$V_{\text{res}} \equiv V_{\text{elec}} - V_{\text{entr}}. \quad (30)$$

We then calculate the system current,  $i$ , from model results, and relate  $V_{\text{res}}$  and  $i$  to the geometric parameter as follows:

$$\frac{L_{\text{eff}}}{S_{\text{eff}}} = \frac{V_{\text{res}} \sigma_M}{i}, \quad (31)$$

where the value of the geometric parameter is independent of the conductivity assigned in our model,  $\sigma_M$ . We performed a parametric study to investigate the effect of changing reservoir characteristic dimension  $D$ , on the geometric parameter  $L_{\text{eff}}/S_{\text{eff}}$ .

To achieve this, we explored six geometries described by the following parameters: channel diameters  $d$  of 20 and 100  $\mu\text{m}$ ; reservoir diameters  $D$  of 2, 6, and 10 mm, reservoir diameter-to-height ratios of unity, and a wire electrode of 0.2 mm diameter. We found that  $L_{\text{eff}}/S_{\text{eff}}$  is insensitive to reservoir and channel diameter. For these conditions, the value of  $V_{\text{res}}$  is dominated by potential loss occurring near the channel entrance. Fig. 4 shows crowding of equipotential and current lines near the channel entrance. Simulations also show that  $L_{\text{eff}}/S_{\text{eff}}$  increases by a factor of approximately 2.5 in changing channel diameter from 100 to 20  $\mu\text{m}$ , indicating a higher Ohmic resistance for the reservoir when connected to the smaller channel. These results suggest that, for this range of dimensions, reservoir potential loss is a strong function of channel diameter but not of reservoir height and diameter.

To further explore the impact of  $V_{\text{res}}$  in electrokinetic systems, we define a parameter,  $\alpha_1$ , describing the ratio of the Ohmic resistance of the reservoirs to the total system resistance, assuming approximately negligible overpotential and equilibrium potential. First, for the case of uniform conductivity, we have:

$$\alpha_1 \approx \frac{2L_{\text{eff}}/S_{\text{eff}}}{2L_{\text{eff}}/S_{\text{eff}} + L/S}. \quad (32)$$

Next, we define a similar parameter,  $\alpha_2$ , describing the ratio of Ohmic resistance of the reservoirs to the total system resistance in the case where the buffer in the anode reservoir has a different conductivity than that in the channel and cathode reservoir:

$$\alpha_2 \approx \frac{(L_{\text{eff}}/S_{\text{eff}})(1 + \gamma)}{(L_{\text{eff}}/S_{\text{eff}})(1 + \gamma) + (L/S)}, \quad (33)$$

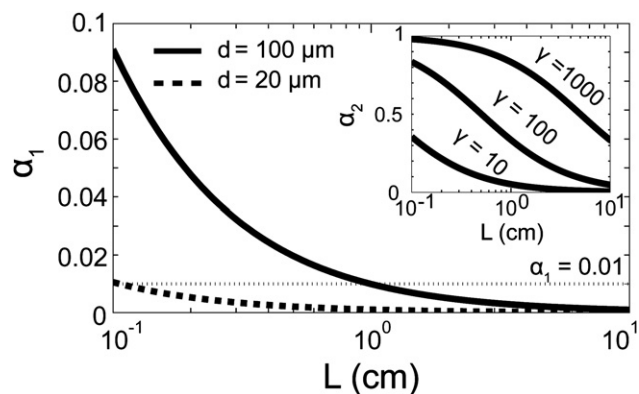


**Fig. 5** The ratio of reservoir to total system resistance,  $\alpha_1$ , as a function of channel length,  $L$ , and channel diameter,  $d$ , for a two-reservoir, one channel device with uniform buffer conductivity. The curves in this plot and inset apply to reservoir characteristic dimensions,  $D$ , from 2 to 10 mm, as the  $L_{\text{eff}}/S_{\text{eff}}$  geometric parameter is unchanged for these  $D$ . Reservoir potential loss remains below 1% of  $V_{\text{app}}$  (dotted grey line) for 20  $\mu\text{m}$  diameter channels, but rises above 1% when  $L < 1$  cm for 100  $\mu\text{m}$  channels. Reservoir losses contribute to a higher fraction of  $V_{\text{app}}$  for wider microchannels. The inset shows ratio of reservoir to total system resistance,  $\alpha_2$ , for the case of uniform cathode reservoir and microchannel electrolyte conductivity, but relatively low anode reservoir conductivity. We plot  $\alpha_2$  versus microchannel length and conductivity ratio,  $\gamma$ , for the case of  $d = 100$   $\mu\text{m}$ . The ratio of reservoir to system resistance,  $\alpha_2$ , increases with conductivity ratio,  $\gamma$ . For a 100  $\mu\text{m}$  diameter channel, reservoir potential drop is approximately 80% of  $V_{\text{app}}$  at  $\gamma = 10^3$ ,  $L = 1$  cm.

where  $\gamma$  is the relevant conductivity ratio,  $\sigma_{cr}/\sigma_{ar}$ . The latter case is relevant to systems which employ non-uniform conductivities such as field amplified sample stacking or isotachopheresis.<sup>57,67</sup> In Fig. 5, we show the parameter  $\alpha_1$  as a function of micro-channel length. For standard electrophoresis chips with uniform conductivity throughout the system and typical geometries ( $L \sim 1\text{--}5$  cm,  $D \sim 2\text{--}10$  mm,  $d < 100$   $\mu\text{m}$ ) the potential drop in both reservoirs remains below 1% of  $V_{app}$  ( $\alpha_1 < 0.01$ ). In typical uniform conductivity systems, reservoir Ohmic potentials are nearly always negligible.

The case of non-uniform system conductivity is very different. Here, reservoir potential loss can be a large percentage of applied potential. In the inset of Fig. 5 we plot  $\alpha_2$  versus channel length, but now for various channel-to-reservoir conductivity ratios,  $\gamma$ . For a 100  $\mu\text{m}$  diameter channel, with  $L = 1$  cm, and a conductivity ratio of  $10^3$ , the potential drop in the anode reservoir approaches 80% of  $V_{app}$ .

Note that the results shown in the inset of Fig. 5 represent a quasi-steady, ideal condition wherein conductivities in each region (channel and reservoir) are well described and uniform. In practice, the problem can be unsteady and strongly dependent on the direction of bulk flow in the system. For example, consider the case where the channel and anode reservoir are filled with high conductivity solution; and the cathode filled with low conductivity solution. If bulk fluid flows from anode to cathode (as in typical electroosmotic flow systems with negative zeta potentials<sup>28</sup>), then high conductivity liquid quickly enters the cathode reservoir from the channel. This should quickly modify the high resistance region near the channel-to-reservoir interface (*cf.* detail view in Fig. 4), quickly lowering the cathode reservoir Ohmic resistance. Such a case should be very different from, say, anode-to-cathode bulk flow with low conductivity only in the anode reservoir. In the latter configuration, a large Ohmic potential drop in the anode reservoir should persist, since it remains filled with only low conductivity.

### General effect of overpotential and equilibrium potential on EK systems

We here investigate the effect of overpotential,  $\eta_a$ , and equilibrium potential,  $E_{eq}$ , on typical DC electrokinetic systems. Generally, these potential losses are on the order of 1 V, and can therefore be neglected for all but low voltage electrokinetic systems. As shown in Fig. 6, at low applied voltage,  $V_{app}$  is dominated by overpotential and equilibrium potential. This regime is called the activation region (with reference to the overpotential and equilibrium potential being the necessary voltage to “activate” the electrode reactions and reach the required Faradaic current). At high applied voltage, Ohmic potential dominates in what we term the Ohmic regime. The real area of the electrode surface,  $S_r$ , is an important parameter for low potential applications, but has negligible effect on  $V_{app}$  at high potentials. This is shown in the inset of Fig. 6 where we plot overpotential versus applied current for a range of real areas. For low DC voltage electrokinetic applications, minimizing power losses can include strategies such as: maximization of  $S_r$ , reduction of  $E_{eq}$  by use of electrodes or electrolytes which result in lower equilibrium potentials,<sup>59</sup> and maximization of  $j_{o,a}$  by use of the best available electrocatalyst as electrode material.<sup>47</sup>

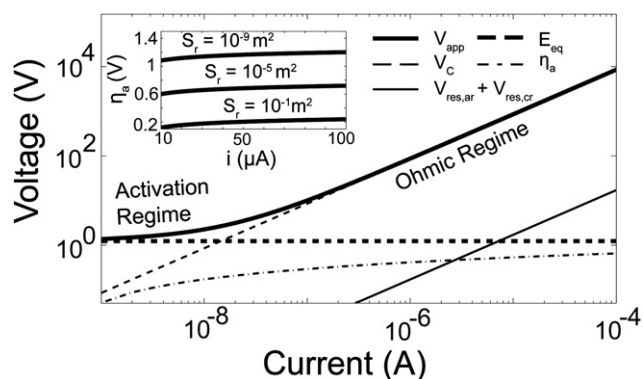


**Fig. 6** A plot of  $V_{app}$  and its constituents versus current at representative parameters for on-chip electrokinetic devices:  $E_{eq} = 1.23$  V,<sup>62</sup>  $\sigma = \sigma_a = \sigma_c = 0.075$  S m<sup>-1</sup>,  $L = 5$  cm,  $d = 100$   $\mu\text{m}$ ,  $D = 2\text{--}10$  mm,  $L_{eff}/S_{eff} = 6380$  m<sup>-1</sup> (from finite element model solution described previously), and  $S_r = 10S_{geom}$  for a 6 mm high and 0.2 mm diameter wire electrode. We used the exchange current density and Tafel slope for the OER on platinum electrodes.<sup>47,63–65</sup> We observe a transition between activation and Ohmic regimes at approximately 10 nA. Operating well into the Ohmic regime, *i.e.* at currents above 1  $\mu\text{A}$ , allows for neglecting overpotential and equilibrium potential losses as they represent a negligible fraction of  $V_{app}$ . The inset shows that over eight orders of magnitude of  $S_r$ , the variation of  $\eta_a$  is order one volt. Therefore  $S_r$  must be precisely determined to model low voltage EK devices, but not for typical high voltage experiments.

### Electrode materials for on chip EK systems

We here focus on electrode materials applicable to on-chip electrokinetic devices, particularly for electrodes introduced at end-channel reservoirs which supply DC current. For these systems, platinum electrodes are most common due to the electrochemical stability and catalytic ability.<sup>47</sup> For typical microfluidic applications, a small length of platinum wire (approximately 1 cm) is connected to the ends of standard high voltage leads (*e.g.*, copper wire). Note that platinum theoretically dissolves at potentials above 1.2 V.<sup>47</sup> Consequently, platinum cannot be considered entirely electrochemically stable. Gencoglu *et al.*<sup>4</sup> performed *in situ* cyclic voltammetry measurements and *ex situ* SEM imaging to visualize platinum oxidation and dissolution at wire electrodes driving electric fields up to approximately 300 V.cm<sup>-1</sup>. They observed both chemical and morphological changes to the platinum wire surface in several electrolytes, including 50 mM Tris-buffered saline and 20 mM HEPES-buffered saline. A major drawback in the use of platinum, especially towards development of commercially available electrokinetic devices, is high cost. Baldwin *et al.*<sup>68</sup> developed sputtered platinum driving electrodes, using platinum layers that are several hundred nanometers thick. Low-cost printed graphite ink electrodes have been successfully implemented as primary driving electrodes in microchip CE devices.<sup>69</sup> However, some carbon-based electrodes have electroactive surfaces and may not be suitable as robust primary electrodes.<sup>70</sup> An interesting set of less expensive materials which merit further investigation for electrokinetic systems are dimensionally stable anodes (DSA), which combine an unstable catalyst and a stabilizing oxide in a thin film supported by a conducting metallic substrate.<sup>71,72</sup>

## Conclusion

We have reviewed of the coupling between acid–base equilibria, electrophoresis, and electrochemistry in typical DC electrokinetic devices. We first presented a brief summary of ion transport by electrophoresis. In particular, we discussed the relation between electrophoretic mobility and species dissociation reactions. We derived a general formulation for the effective electrophoretic mobility of a weak electrolyte with an arbitrary number of dissociations. We also discussed the departure of mobility data from infinite dilution approximations. The latter included presentation of a Pitts model for ionic strength correction of the ideal, infinite dilution mobility. As an illustrative example, we showed the variation of predicted effective electrophoretic mobility (based on known  $pK_a$  and fully-ionized mobility data) for fluorescein as a function of pH and ionic strength.

We presented an analysis of electrode reactions on buffer systems in typical microfluidic electrokinetic experiments. We derived a closed form expression for the temporal variation of pH in well-stirred reservoirs for buffers composed of a weak electrolyte and a strong titrant. We showed that pH can significantly change if the electrolyte is not well buffered and/or the reservoirs are not large enough for the current and time frame of interest. We showed that the case of the anode and cathode are very different and depend on whether a weak acid or a weak base are used for buffering. We also derived a set of non-dimensional parameters useful in estimating pH effects in reservoirs.

We then described the effects of electrode reactions on microfluidic electrokinetic systems. We first discussed electrolysis. The nature of electrode reactions depends on electrode polarity and electrolyte pH (*cf.* Table 2). We then presented a simple model to describe potential applied to electrokinetic system electrodes in terms of potential drop across channel lengths and several sources of potential losses. We decomposed the applied potential into overpotential (using a Tafel formulation), equilibrium potential, the potential drop within end-channel reservoirs, and the potential drop over long, thin channels. More practically, we performed three dimensional simulations to estimate the effects of channel and reservoir dimensions on the potential loss in reservoirs. We showed that in a typical electrokinetic device with reservoirs of order 1  $\mu\text{L}$  to 1 mL and characteristic channel dimensions below 100  $\mu\text{m}$ , the potential drop in the reservoirs is negligible for channels longer than 1 cm. We also showed that non-homogeneous buffer systems can increase potential drop in the reservoirs, and high channel-to-reservoir conductivity ratios can yield reservoir potential drops representing a significant fraction of applied potential. We briefly discussed electrode materials and their potential application to microfluidic electrokinetics. We also suggested various methods for managing bubble generation and lowering overpotential in electrokinetic systems.

Overall, the presentations serve as an introduction to the principles associated with the coupling between electrochemistry, acid–base equilibrium, and electromigration phenomena. We argue that a basic understanding of this coupling is critical to the design, analysis, testing, and optimization of electrokinetic microfluidic systems.

## Acknowledgements

Matthew Suss was supported by the FQRNT fellowship. We gratefully acknowledge the support of the DARPA MTO sponsored SPAWAR Grant N66001-09-1-2007. We thank Thomas F. Jaramillo and Moran Bercovici for insightful discussions and comments.

## References

- 1 B. J. Kirby and E. F. Hasselbrink, *Electrophoresis*, 2004, **25**, 187–202.
- 2 K. D. Lukacs and J. W. Jorgenson, *Journal of High Resolution Chromatography & Chromatography Communications*, 1985, **8**, 407–411.
- 3 S. H. Yao and J. G. Santiago, *Journal of Colloid and Interface Science*, 2003, **268**, 133–142.
- 4 A. Gencoglu and A. Minerick, *Lab on a Chip*, 2009, **9**, 1866–1873.
- 5 G. J. M. Bruin, *Electrophoresis*, 2000, **21**, 3931–3951.
- 6 L. Bousse, C. Cohen, T. Nikiforov, A. Chow, A. R. Kopf-Sill, R. Dubrow and J. W. Parce, *Annual Review of Biophysics and Biomolecular Structure*, 2000, **29**, 155–181.
- 7 A. Persat, R. Chambers and J. G. Santiago, *Lab on a Chip*, 2009, DOI: 10.1039/b906465f.
- 8 R. A. Robinson and R. H. Stokes, *Electrolyte solutions, the measurement and interpretation of conductance, chemical potential, and diffusion in solutions of simple electrolytes*, Butterworths Scientific Publications, London, 1959.
- 9 J. P. Landers, *Handbook of Capillary and Microchip Electrophoresis and Associated Microtechniques*, Taylor & Francis Group, LLC, Boca Raton, FL, 2008.
- 10 F. M. Everaerts, J. L. Beckers and T. P. E. M. Verheggen, *Isotachopheresis: theory, instrumentation, and applications*, Elsevier Scientific Pub. Co., Amsterdam, 1976.
- 11 I. N. Levine, *Physical chemistry*, McGraw-Hill, London, 2003.
- 12 D. M. Li, S. L. Fu and C. A. Lucy, *Analytical Chemistry*, 1999, **71**, 687–699.
- 13 V. Hruska and B. Gas, *Electrophoresis*, 2007, **28**, 3–14.
- 14 L. M. Hjelmeland and A. Chrambach, *Electrophoresis*, 1982, **3**, 9–17.
- 15 P. Bednar, Z. Stransky, J. Sevcik and V. Dostal, *Journal of Chromatography A*, 1999, **831**, 277–284.
- 16 L. G. Longworth, *Journal of the American Chemical Society*, 1932, **54**, 2741–2758.
- 17 L. G. Longworth, *Journal of the American Chemical Society*, 1935, **57**, 1185–1191.
- 18 C. X. Cao, *Journal of Chromatography A*, 1998, **813**, 173–177.
- 19 C. X. Cao, *Progress in Natural Science*, 1999, **9**, 602–609.
- 20 J. Kielland, *Journal of the American Chemical Society*, 1937, **59**, 1675–1678.
- 21 M. Jaros, K. Vcelakova, I. Zuskova and B. Gas, *Electrophoresis*, 2002, **23**, 2667–2677.
- 22 C. W. Whang and E. S. Yeung, *Analytical Chemistry*, 1992, **64**, 502–506.
- 23 N. O. Mchedlov-Petrosyan, V. I. Kukhtik and V. I. Alekseeva, *Dyes and Pigments*, 1994, **24**, 11–35.
- 24 D. Milanova, R. D. Chambers and J. G. Santiago, 2009, unpublished work.
- 25 M. M. Martin and L. Lindqvist, *Journal of Luminescence*, 1975, **10**, 381–390.
- 26 H. Diehl and R. Markuszewski, *Talanta*, 1989, **36**, 416–418.
- 27 M. Bercovici, S. K. Lele and J. G. Santiago, *Journal of Chromatography A*, 2009, **1216**, 1008–1018.
- 28 R. F. Probstein, *Physicochemical Hydrodynamics: An Introduction*, Second edn., John Wiley & Sons, Inc., New York, 1994.
- 29 H. S. Harned and R. L. Nuttall, *Journal of the American Chemical Society*, 1949, **71**, 1460–1463.
- 30 H. Galster, *pH measurement: Fundamentals, Methods, Applications, Instrumentation*, VCH, New York, 1991.
- 31 J. N. Butler and D. R. Cogley, *Ionic equilibrium: solubility and pH calculations*, Wiley, New York, NY, 1998.
- 32 B. Alberts, *Molecular biology of the cell. Reference edition*, Garland Science, New York, 2008.
- 33 M. S. Bello, *Journal of Chromatography A*, 1996, **744**, 81–91.

- 34 H. Corstjens, H. A. H. Billiet, J. Frank and K. Luyben, *Electrophoresis*, 1996, **17**, 137–143.
- 35 I. Rodriguez and N. Chandrasekhar, *Electrophoresis*, 2005, **26**, 1114–1121.
- 36 M. Macka, P. Andersson and P. R. Haddad, *Analytical Chemistry*, 1998, **70**, 743–749.
- 37 T. Revermann, S. Gotz, J. Kunemeyer and U. Karst, *Analyst*, 2008, **133**, 167–174.
- 38 E. C. Potter, *Electrochemistry: Principles and applications*, Cleaver-Hume Press, London, 1956.
- 39 T. Erdey-Gruz, *Kinetics of electrode processes*, Hilger, London, 1972.
- 40 A. V. Stoyanov and J. Pawliszyn, *Analyst*, 2004, **129**, 979–982.
- 41 J. P. Schaeper and M. J. Sepaniak, *Electrophoresis*, 2000, **21**, 1421–1429.
- 42 H. E. Schwartz, M. Melera and R. G. Brownlee, *Journal of Chromatography A*, 1989, **480**, 129–139.
- 43 A. Oki, Y. Takamura, Y. Ito and Y. Horiike, *Electrophoresis*, 2002, **23**, 2860–2864.
- 44 M. A. Kelly, K. D. Altria and B. J. Clark, *Journal of Chromatography A*, 1997, **768**, 73–80.
- 45 C. K. Harnett, J. Templeton, K. A. Dunphy-Guzman, Y. M. Senousy and M. P. Kanouff, *Lab on a Chip*, 2008, **8**, 565–572.
- 46 J. Buehrle, S. Herminghaus and F. Mugele, *Physical Review Letters*, 2003, **91**, 086101.
- 47 J. O. M. Bockris, A. K. N. Reddy and M. Gamboa Aldeco, *Modern Electrochemistry: Fundamentals of Electrode Processes*, Springer, 2000.
- 48 C. Gabrielli, F. Huet, M. Keddam, A. Macias and A. Sahar, *Journal of Applied Electrochemistry*, 1989, **19**, 617–629.
- 49 J. Eigeldinger and H. Vogt, *Electrochimica Acta*, 2000, **45**, 4449–4456.
- 50 W. E. Morf, O. T. Guenat and N. F. de Rooij, *Sensors and Actuators B: Chemical*, 2001, **72**, 266–272.
- 51 A. Brask, J. P. Kutter and H. Bruus, *Lab on a Chip*, 2005, **5**, 730–738.
- 52 M. Moini, P. Cao and A. J. Bard, *Analytical Chemistry*, 1999, **71**, 1658–1661.
- 53 D. Kohlheyer, J. C. T. Eijkel, S. Schlautmann, A. van den Berg and R. B. M. Schasfoort, *Analytical Chemistry*, 2008, **80**, 4111–4118.
- 54 P. K. Dasgupta and S. Liu, *Analytical Chemistry*, 1994, **66**, 1792–1798.
- 55 A. Brask, D. Snakenborg, J. P. Kutter and H. Bruus, *Lab on a Chip*, 2006, **6**, 280–288.
- 56 Y. Xu, J. W. Shen, J. L. Lu and Z. Y. Wen, *J. Micro-Nanolithogr. MEMS MOEMS*, 2007, **6**, 7.
- 57 M. C. Breadmore and P. R. Haddad, *Electrophoresis*, 2001, **22**, 2464–2489.
- 58 L. M. Fu and R. J. Yang, *Electrophoresis*, 2003, **24**, 1253–1260.
- 59 K. A. D. Guzman, R. N. Karnik, J. S. Newman and A. Majumdar, *Journal of Microelectromechanical Systems*, 2006, **15**, 237–245.
- 60 Y. Takamura, H. Onoda, H. Inokuchi, S. Adachi, A. Oki and Y. Horiike, *Electrophoresis*, 2003, **24**, 185–192.
- 61 Y. F. Chen, M. C. Li, Y. H. Hu, W. J. Chang and C. C. Wang, *Microfluidics and Nanofluidics*, 2008, **5**, 235–244.
- 62 A. J. Bard, L. R. Faulkner, *Electrochemical Methods: Fundamentals and Applications*, John Wiley & Sons Inc., 2001.
- 63 V. I. Birss and A. Damjanovic, *Journal of The Electrochemical Society*, 1983, **130**, 1694–1699.
- 64 B. V. Tilak and C. P. Chen, *Journal of Applied Electrochemistry*, 1993, **23**, 631–640.
- 65 S. S. B. Viswanathan, A. V. Ramaswamy, *Catalysis: Principles and Applications*, CRC Press, 2002.
- 66 S. Trasatti and O. A. Petrii, *Pure Appl. Chem.*, 1991, **63**, 711–734.
- 67 S. Song and A. K. Singh, *Analytical and Bioanalytical Chemistry*, 2006, **384**, 41–43.
- 68 R. P. Baldwin, T. J. Roussel, M. M. Crain, V. Bathlagunda, D. J. Jackson, J. Gullapalli, J. A. Conklin, R. Pai, J. F. Naber, K. M. Walsh and R. S. Keynton, *Analytical Chemistry*, 2002, **74**, DOI: 10.1021/ac011188n|UNSP AC011188N.
- 69 C. G. Koh, W. Tan, M. Q. Zhao, A. J. Ricco and Z. H. Fan, *Analytical Chemistry*, 2003, **75**, 4591–4598.
- 70 A. A. Franco and M. Gerard, *Journal of The Electrochemical Society*, 2008, **155**, B367–B384.
- 71 S. Trasatti, *Electrochimica Acta*, 2000, **45**, 2377–2385.
- 72 C. Comninellis and G. P. Vercesi, *Journal of Applied Electrochemistry*, 1991, **21**, 335–345.